ARTICLE

Towards rational catalyst design: Boosting rapid prediction of transition-metal activity by improved scaling relations

Received 00th January 20xx,
Accepted 00th January 20xx

DOI: 10.1039/x0xx00000x

Yalan Wang,[‡a] Ling Xiao,[‡b] Yanying Qi,[a] Mehdi Mahmoodinia,[a] Xiang Feng,[a] Jia Yang,[a] Yi-An Zhu*[b] and De Chen*[a]

Understanding scaling relations of adsorption energies and activation energies greatly facilitate the computational catalyst design. To reduce the computational cost and guarantee the efficiency, improved scaling relations are advocated in this study to fast acquire energetics for transition metal surface reactions, further to rapidly and effectively map the activity of transition-metal catalysts. The overall catalytic activity for surface reactions between C, H and O containing species can be related backed to the adsorption energies, using C, H and O binding energies as descriptors via the improved scaling relations. The UBI-QEP (unity bond index-quadratic exponential potential) method, one of scaling relations to estimate adsorption energies from descriptors, is significantly improved by taking into account the changes in A-B bond index during the adsorption and the molecular structure of adsorbed species using density functional theory (DFT) data as a benchmark. The improved UBI-QEP approach can satisfactorily predict the DFT (BEEF-vdW) and experimental adsorption energies. DFT calculations with BEEF-vdW functional are also employed for establishing the BEP (Brønsted-Evans-Polanyi) relationships, scaling relations to correlate reaction heats with activation energies, for C-H, C-O, C-C, O-H bond cleavages and recombination. The capability of improved UBI-QEP + BEP approach is tested as a generic framework to map the activity trend for steam methane reforming (a probe reaction) through microkinetic modeling. The results demonstrate that our approach reduces the computational cost in six orders of magnitude, while maintains a reasonable degree of accuracy as compared to the DFT (BEEF-vdW) and experiments.

Introduction

Microkinetic modeling-aided design of catalysts is a major topic for developing novel catalysts without intensive empirical testing, especially for research on transition metal catalysts.[1–5] The model serves as a measure to probe reaction mechanism and predict the activity and selectivity of catalysts.[6] Theoretical chemistry provides a feasible way to estimate input parameters (surface energetics) of a microkinetic model. Among others, density functional theory (DFT) calculation[7–12] is currently the most prevalent approach. However, DFT calculations are normally complex, time-consuming, and computationally expensive because hundreds of elementary steps may be involved in a real process under different structures and surface coverage.[13, 14] Consequently, it is not efficient to calculate all reaction steps only based on first-principles computation. Simpler and efficient method is therefore highly desired to rapidly determine energetics for a preliminary catalyst screening.

The linear scaling relations (LSRs) introduced by Nørskov and co-workers[15] effectively correlate a partially hydrogenated adsorbate (AH_x) binding energy to atomic (A) binding energy over transition-metal surfaces, which greatly facilitate the computational catalyst design. The LSRs can be derived from bond order conservation, currently knowns as unity bond index-quadratic exponential potential (UBI-QEP) method.[16-19] UBI-QEP provides approaches to characterize complex species ($C_xH_yO_z$) and is thus advocated herein for prediction of binding energies.[20-24] The binding energies of atomic adsorbates A and B (Q_A, Q_B) are descriptors to estimate the binding energy of adsorbate AB (Q_{AB}).[25] In other words, an enormously complex system involving hundreds of adsorbates can be simplified as one that is only related to several atomic bindings via the UBI-QEP method. With the much less demanding computation achieved, a major problem encountered is that the accuracy of this method is in general uncertain, which seriously limits its application.[14] In this situation, utilizing DFT values as a systematic benchmark to assess the limitations of UBI-QEP for representative adsorbates and to propose improved methods is of great significance. However, few attentions have been focused on this.[14, 26, 27] Herein, we make an effort to build the optimization process adopting DFT data to improve the UBI-QEP model, so as to keep the model with a reasonable degree of accuracy towards binding energies for studied intermediates on metal surfaces of interest. The improved UBI-QEP model will be further utilized to predict the binding energies of other

[a] Department of Chemical Engineering, Norwegian University of Science and Technology, 7491 Trondheim, Norway. Email: de.chen@ntnu.no
[b] UNILAB, State Key Laboratory of Chemical Engineering, East China University of Science and Technology, Shanghai 200237, China. Email: yanzhu@ecust.edu.cn

† Electronic Supplementary Information (ESI) available: Standard UBI-QEP method, adsorption configurations, detailed classification of BEP relationships, TSS correlations, and microkinetic modeling details. See DOI: 10.1039/x0xx00000x

‡ These authors contributed equally to this work

intermediates or on new metal surfaces that have no available DFT values.

Another commonly used scaling relation in computational catalysis is Brønsted-Evans-Polanyi (BEP) relationship,[28, 29] which classically links activation barriers E_a (kinetics) with enthalpy changes ΔH (thermodynamics),

$$E_a = \alpha_0 \Delta H + \beta_0 \quad (1)$$

Where the slope, α_0, is a measure of the earliness or lateness of the transition state and implies its possible geometry, i.e. the value close to unity indicates a late transition state (product-like).[30, 31] Along the BEP line, a displacement of ΔH reflects the electronic effect (d-band center), and a change of β_0 corresponds to the surface geometrical effect.[32] These correlation parameters rely extremely on the researched data. To date, despite a large amount of research towards the BEP relationship,[30, 33–36] little work has systematically investigated the linear relation with regard to C-, H-, and O-containing reactions on the basis of large amount of transition-metal surfaces. Understanding this would be helpful for rapidly acquiring activation energies and undoubtedly valuable for reactions involving hydrocarbons, alcohols and acids.

Here we develop improved scaling relations (UBI-QEP + BEP) to quickly generate the energetics for transition metal surface reactions, which can be utilized for rational design of novel catalysts through microkinetic modeling, as well as in mechanistic studies. The C-, O-, and H-containing species and reactions are studied due to their significant industrial applications such as in Fischer-Tropsch synthesis and steam reforming reactions. Computational catalyst prediction is performed based on this idea: Descriptors → Adsorption energies → Activation energies → Activity. The C-, O-, and H-metal binding energies are descriptors to identify the adsorption energies via improved UBI-QEP method, and the activation energies are acquired by combination of BEP relationships. The microkinetic modeling is subsequently conducted over Ni, Rh, Pt, Pd, Cu, Fe, Ru, and Co surfaces to predict their catalytic activity and screen their efficiency. To refine the model, the kinetic parameters of rate-determining steps are calculated by DFT computations.[13] This work offers a new possibility for model-aided catalyst prediction, with which we can gain better understanding of reaction mechanism and achieve the goal of rational catalyst design.

Results and discussion

General

The scheme of descriptor-based microkinetic modeling is displayed in Figure 1. Calculations of energetics with DFT exhibit reasonable accuracy but expensive computational cost. In contrast, the improved scaling relations (UBI-QEP + BEP) are computationally cheap but show uncertain accuracy. To guarantee the accuracy, DFT calculations with the BEEF-vdW functional, performed on the Pt(111), Pd(111), Rh(111), Cu(111), Ni(111), Fe(110), Ru(0001), and Co(0001) surfaces, are used as a benchmark to improve the UBI-QEP method and obtain BEP relationships. The standard UBI-QEP equations are given in Table S1 (See Supplementary Information Part S1), which indicate that M_n-A binding energy (Q_A), coordination number (n), and bond energy (D_{AB}) are crucial parameters for obtaining the adsorption heats. Several recommended M_n-A binding energies (A is C, O, H) have been provided by Shustorovich and co-workers.[27, 37, 38] Some coordination numbers and bond energies are also available from prior studies.[19, 39] Given that it is difficult to acquire all desired data in literature, DFT calculations are attempted here to uniformly identify Q_A, n and D_{AB} values.

BEP relationships for the C-O, C-C, C-H, and O-H bond cleavage and recombination reactions over transition metals are systematically established based on a large database of DFT values. The adsorption energies and activation barriers are predicted rapidly by adopting the DFT-corrected UBI-QEP model and the BEP relationships. These energies are then utilized in the microkinetic model for the first step of catalyst design to quickly screen highly active transition metals, with only C-, H-, and O-metal binding energies as descriptors.[40, 41] On the other hand, the microkinetic model can efficiently aid the mechanism studies, searching for a dominant reaction pathway and the rate-determining step. Subsequent kinetic expression extraction and model training with experimental results can be further applied to catalyst design. In this study, we mainly focus on estimating the surface energetics and preliminary catalyst prediction; the detailed microkinetic analysis for catalyst design will be introduced in the future work.

Steam methane reforming (SMR) is taken as a probe reaction for microkinetic modeling. Six different models (DFT, DFT+BEP, UBI-QEP+BEP, and three refined models using DFT calculated energetics of rate-determining steps) are built to compare with experiments and with each other. This process provides a tool for testing data accuracy and verifying the applicability of the improved scaling relations. The refined models are highly recommended for screening the novel materials.

Determination of D_{AB}

Bond energy, D_{AB}, has three types of formalisms according to different M_n-AB binding situation.[19, 39] For $\eta^1\mu_n$ coordination, e.g., AB adsorbs perpendicular to a metal surface with A end down, D_{AB} is the enthalpy of AB bond breaking reaction in the gas phase, namely the total bond energy between A and the rest of molecule AB in the gas phase. B can be atoms, groups of atoms or radicals. For $\eta^2\mu_n$ coordination, D_{AB} is the total gas-phase bond energy of AB or bond energy between A and B in the gas phase. Under this definition, D_{AB} value is related to total gas-phase bond energy of AB, A and B, as well as coordination environment.

The total gas-phase bond energy (D) is estimated by DFT (BEEF-vdW) calculations in this work, described as:

$$D = E_{C_xH_yO_z} - xE_C - yE_H - zE_O \quad (2)$$

Where E_{CxHyOz}, E_C, E_H, and E_O are the DFT calculated total energies of gas-phase $C_xH_yO_z$, C, H, and O, respectively; x, y and z are the numbers of C, H and O atoms in $C_xH_yO_z$. The DFT calculated total gas-phase bond energy (D) against suggested UBI-QEP values that taken from Storsæter' work[39] is displayed

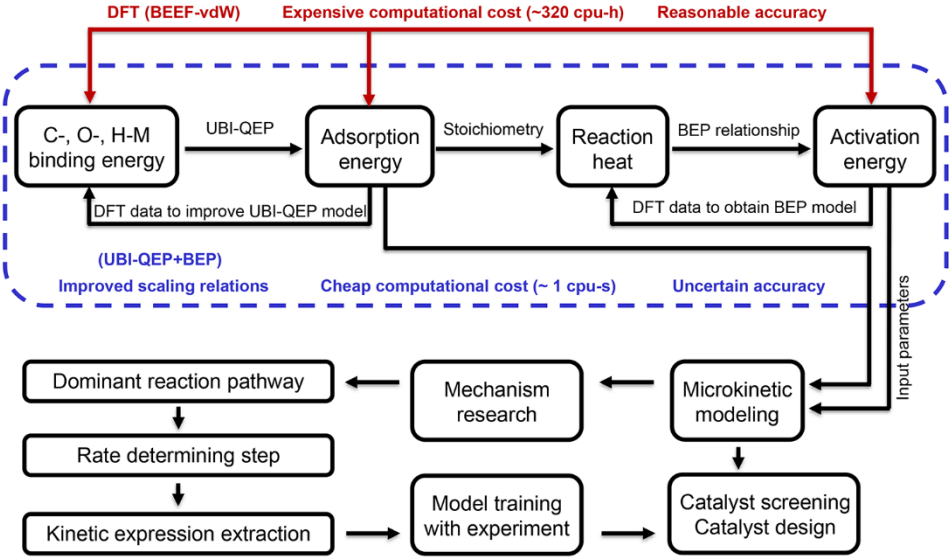

Figure 1. Scheme of descriptor-based microkinetic modeling. Calculations of energetics with DFT (BEEF-vdW) exhibit reasonable accuracy but expensive computational cost. In contrast, the improved scaling relations are computationally cheap but show uncertain accuracy. C-, O-, and H-M binding energies are three descriptors of the improved scaling relations, with which adsorption energies are estimated by UBI-QEP method, activation energies are obtained with BEP relationships. The estimated energies are employed as input parameters to conduct microkinetic modeling and mechanism research, further to aid catalyst design.

in Figure S1, which demonstrates a particularly good relationship, proving the accuracy and validity of DFT values with the BEEF-vdW functional. Bond energy (D_{AB}) is calculated from DFT estimated D value and compared with literature results.[39] The good scaling relation (Figure S1, black squares) indicates that using DFT computations to estimate bond energy is a feasible approach; it is quick and easy to get all desired values.

Prediction of adsorption heats

Atomic M_n-A binding energy (Q_A) is the most important descriptor of adsorption heats via UBI-QEP method. In order to correspond with D_{AB}, DFT calculated Q_A is applied in this study. Therefore, heat of adsorption is first predicted using the standard UBI-QEP equations and with the DFT estimated Q_A, n, and D_{AB} as input parameters. Here n is determined from adsorption configurations by DFT calculations (See Supplementary Information Part S1). The predicted adsorption heats show, however, a poor relationship with the corresponding values from DFT (BEEF-vdW) calculations, as shown in Figure 2a. In this Figure, binding energies (absolute value of adsorption heats) estimated by standard UBI-QEP method are plotted against the DFT values for different species on the close-packed Co, Ru, Fe, Ni, Cu, Rh, Pd and Pt surfaces. For strong binding, the standard UBI-QEP methods underestimate the values with respect to the DFT results. The stronger the binding energy, the greater the underestimation. For weak binding, however, overestimation of binding energies occurs in UBI-QEP model against DFT references. As a result, it is necessary to improve the accuracy of the UBI-QEP approach in order to further utilize it in the prediction of activation barrier.

The fact that UBI-QEP method underestimates the binding energy of strongly bounded species has been reported in previous studies.[26, 27] Higher binding energy corresponds to shorter distance between adsorbate and the metal surface. Vesselli et al.[26] studied ethanol decomposition on the Pt(111) surface with the UBI-QEP method and compared the results with those obtained by DFT, concluding that binding energies for metal-adsorbate with a distance shorter than 2.2 Å were underestimated in the UBI-QEP model. Because the UBI-QEP model is based on the assumption of unity bond index, and the definition of bond index is polynomial functions of exponential, for short bond distance, charge densities will overlap with profiles that deviate from an exponential form,[42] resulting in the error of the UBI-QEP model. The higher the binding energy, the shorter the bond length, the larger the error caused by UBI-QEP model. Moreover, assumptions and simplifications imposed in the system have a major effect on the reduced accuracy. In the original UBI-QEP method, the total energy of a strong M_n-AB binding system ($\eta^1\mu_n$ coordination, with A bound to metal) is expressed as:

$$E_{AB}\left(x_A, x_{AB}\right) = Q_A\left(x_A^2 - 2x_A\right) + D_{AB}\left(x_{AB}^2 - 2x_{AB}\right) \quad (3)$$

Where x_A, x_{AB} are bond index of A and B, respectively. With the UBI conservation:

$$x_A + x_{AB} = 1 \quad (4)$$

Constrained minimization of UBI-QEP energy leads to

$$x_A = \frac{Q_A}{Q_A + D_{AB}} \quad (5)$$

The binding energy of AB calculated by standard UBI-QEP method is given as

$$Q_{AB} = -E - D_{AB} = \frac{Q_A^2}{Q_A + D_{AB}} \quad (6)$$

Here, D_{AB} is AB bond dissociation energy in the gas phase. When M_n-AB binding is not very strong (< 3 eV), the adsorption does not significantly alter the bond length of A-B which is similar to the one in the gas phase. Therefore, AB bond energy in M_n-AB binding in Eq. (6) system is approximated to the same as the gas phase D_{AB}. For the case with very strong M_n-AB binding (> 5 eV), however, the adsorption modifies the A-B bond length and results in a change in the AB bond energy (D_{AB}) with the bond index as shown in Eq. (7). The adsorption energy is calculated by

$$Q_{AB} = -E - D_{AB}\left(2x_{AB} - x_{AB}^2\right) = \frac{Q_A^2}{Q_A + D_{AB}} + \frac{Q_A^2 D_{AB}}{\left(Q_A + D_{AB}\right)^2} \quad (7)$$

Which is one of improved UBI-QEP equations in this work. The latter part of above equation accounts the contribution of changes in the molecular structure to the adsorption energy induced by strong adsorption. All modified UBI-QEP equations for adsorption heats are summarized in Table 1.

For mediate-strong adsorption (3 eV < Q_{AB} < 5 eV), the contribution to the adsorption heat due to change in the AB bond energy (D_{AB}) with the bond index is also mediate. We introduce a factor of σ in the Eq. (9) in Table 1, which is between 0 (Q_{AB} < 3eV) and 1 (Q_{AB} > 5eV). From the best fitting to the DFT data, σ is about 1/3 (Possibly a value in range of 0.33-0.4).

In contrast to strong bindings, the standard UBI-QEP model overestimates the binding energies for weak bindings, as shown in Figure 2a. According to the UBI-QEP assumptions, diatomic molecules (polyatomic molecules) are modeled as quasi-atoms (quasi-diatomic molecules). In the case of M-A-B mono-coordination (AB is perpendicularly adsorbed on metal surface, with A end down and B end up), the M_n-AB binding occurs via attractive M_n-A interaction and repulsive M_n-B interaction from quantum chemical analysis.[38] If the M_n-A interaction is much stronger than that of M_n-B, the latter could be ignored. For

Table 1 Modified UBI-QEP equations for calculation of adsorption heats

Eq. no.	Case	Equation
(8)[a]	Atomic chemisorption M_n-A binding ($\eta^1\mu_n$ coordination)	$Q_A = (2 - \frac{1}{n})Q_{0A}$
(9)[b]	Strong M_n-AB binding ($\eta^1\mu_n$ coordination)	
	σ =0 Q_{AB} < 3 eV	$Q_{AB} = \frac{Q_A^2}{Q_A + D_{AB}} + \sigma * \frac{Q_A^2 D_{AB}}{\left(Q_A + D_{AB}\right)^2}$
	σ =1/3 3 eV < Q_{AB} < 5 eV	
	σ =1 Q_{AB} > 5 eV	
(10)[b]	Weak M_n-AB binding ($\eta^1\mu_n$ coordination)	$Q_{AB,n} \approx \frac{1}{\beta} * \frac{Q_{0A}^2}{\left(Q_{0A}/n\right) + D_{AB}}$ for $D_{AB} > \frac{n-1}{n}Q_{0A}$
(11)[b]	Intermediate M_n-AB binding via A ($\eta^1\mu_n$ coordination)	$Q_{AB} = \frac{1}{2}\left[\frac{Q_A^2}{Q_A + D_{AB}} + \frac{Q_{0A}^2}{\left(Q_{0A}/n\right) + D_{AB}}\right]$
(12)[c]	Symmetric molecules (CO_2, H_2) ($\eta^2\mu_n$ coordination)	$Q_{AB} = \frac{9Q_{0A}^2}{6Q_{0A} + 16D_{AB}}$
(13)[c]	Complex symmetric species ($AB_{\beta'}$-$AB_{\beta'}$) ($\eta^2\mu_n$ coordination)	$Q_{AB} = \frac{\alpha}{2\beta'} * \frac{9Q_A^2}{6Q_A + 16D_{AB}}$
(14)[d]	Non-symmetric species (AX_m-$BY_{m'}$) ($\eta^2\mu_n$ coordination)	$Q_{AX_m - BY_{m'}} = Q_{A-M} + Q_{B-M}$

[a]Q_A is the M_n-A binding energy (one A atom binds to n metal atoms), which is estimated from experiments or DFT calculations; Q_{0A} is M-A two-center bond energy at equilibrium distance; n is coordination number, namely the total number of metal atoms with which A binds.

[b]AB binds to a metal surface via only one atom A ($\eta^1\mu_n$ coordination), D_{AB} is the total bond energies between A and the rest of molecule AB in gas-phase. β is the number of atoms (B) in the molecule (AB) to which A binds.

[c]AB binds to a metal surface via two A atoms ($\eta^2\mu_n$ coordination), D_{AB} is the total bond energies between A and the rest of molecule AB in gas-phase. α means the valence of A in radical $AB_{\beta'}$, $2\beta'$ is the total number of B in the molecule (B could be one atom or group).

[d]AB binds to a metal surface via both A and B ($\eta^2\mu_n$ coordination), D_{AX} is total bond energies between A and the rest of molecule AX_m in gas-phase; D_{BY} is total bond energies between B and the rest of $BY_{m'}$ in gas-phase.

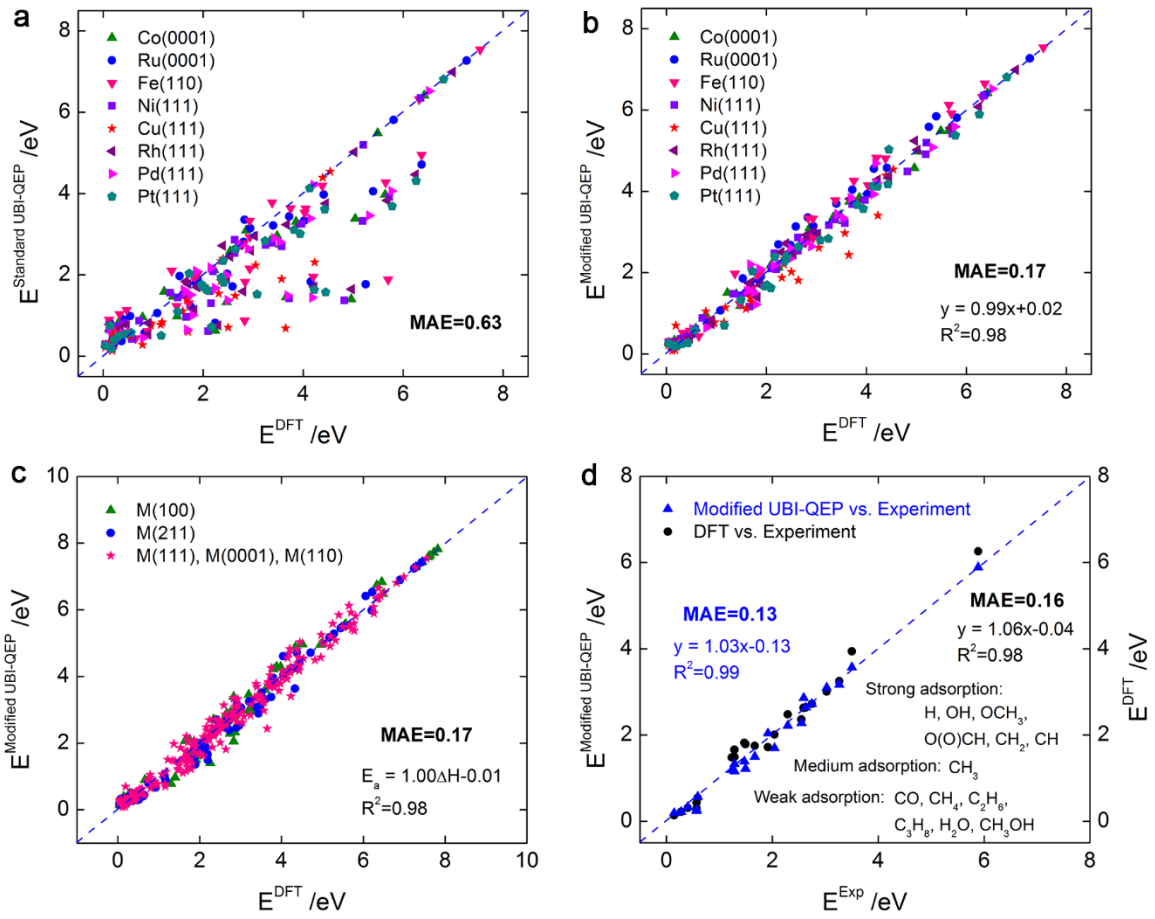

Figure 2. a, Standard UBI-QEP estimated binding energies (absolute value of adsorption energies) with respect to DFT (BEEF-vdW) values on the most close-packed surfaces of Co, Ru, Fe, Ni, Cu, Rh, Pd and Pt; b, Modified UBI-QEP estimated binding energies against DFT (BEEF-vdW) calculated ones on the most close-packed surfaces of Co, Ru, Fe, Ni, Cu, Rh, Pd and Pt; c, Modified UBI-QEP estimated binding energies versus DFT (BEEF-vdW) results on M(100), M(211), M(111), M(0001) and M(110) surfaces. M represents for Co, Fe, Pt, Pd, Ru, Rh, Ni, Cu, Ag, and Au; d, Modified UBI-QEP method and DFT (BEEF-vdW) estimated binding energies (eV) of CO, CH_4, C_2H_6, C_3H_8, H_2O, CH_3OH, CH_3, CH_2, CH, H, OH, OCH_3 and O(O)CH against experimental results.[43–45]

mono-A-coordination, neglecting the weak repulsive M_n-B contribution is a fundamental assumption during UBI-QEP formula derivation, which is relatively accurate for strong binding species due to much stronger M_n-A effect. However, this assumption overestimates the binding energies of weakly bounded species, since the repulsive contribution from M_n-B is not negligible as compared to the weak attractive M_n-A interaction. The more the number of atoms (B) bound to A, the larger the overestimation of binding energies estimated by standard UBI-QEP. By introducing a factor of $1/\beta$ in Eq. (10), Table 1, the UBI-QEP model estimates the adsorption heat for weak M_n-AB interaction relatively well. β is the number of atoms (B) in the molecule (AB) to which A binds.

Since the UBI-QEP estimated binding energies for medium bounded species (CH_3, CH_3CH_2) with $\eta^1\mu_n$ coordination have a good fitting with that of the DFT calculations, no modifications were made for these species. The standard UBI-QEP method for calculation of medium binding is identified by interpolation between strong binding and weak binding equations, and 0.5 is used as the empirical parameter, namely average as the simplest interpolation. The good fitting might be caused by the neutralization of underestimation of strong binding and overestimation of weak binding. Therefore, the original UBI-QEP equation is still applied in this situation, shown as Eq. (11) in Table 1.

All three aforementioned cases are suitable for $\eta^1\mu_n$ coordination, i.e., AB binds to a metal surface via only atom A. For more complex species, the M_n-AB can bind via both A and B to the metal surfaces ($\eta^2\mu_n$ coordination). Considering simple symmetric molecules like H_2 and CO_2, adsorption heats can be well predicted by the standard UBI-QEP model Eq. (12) in Table 1. However, for more complex symmetric molecules, such as CHCH, CH_2CH_2, and CH_3CH_3, a factor similar to the weak M_n-AB binding ($\eta^1\mu_n$ coordination) is introduced into the Eq. (13) in Table 1, reflecting the effect of extra coordination (B) to the adsorption heat. The $AB_{\beta'}$ -$AB_{\beta'}$ adsorbate binds to the metal surface via A atoms, and B can be an atom or a group of atoms. D_{AB} is the total bond energy between A and the remainder of

molecule in the gas phase. $2\beta'$ is the total number of B in the molecule. The physical meaning of $2\beta'$ is similar to the parameter β in Eq. (10), which is used to describe the repulsive M_n-B interaction. α refers to the available valence for atom A in the radical $AB_{\beta'}$, which is 3 for CH, 2 for CH_2, and 1 for CH_3. The more available valence the atom A has, the higher the binding energy to the surface.

Another case for $\eta^2\mu_n$ coordination corresponds to non-symmetric molecules. The original UBI-QEP formulas for estimating adsorption heats in this case are very complicated, as in Eq. (S9) and (S11) in Table S1. In order to simplify the expression, we assume that the total binding energy of $\eta^2\mu_n$ coordination equals to sum of the two $\eta^1\mu_n$ coordination binding energies, shown as Eq. (14) in Table 1. $Q_{A\text{-}M}$ and $Q_{B\text{-}M}$ are binding energies of M_n-AX_m and M_n-$BY_{m'}$ fragments in such an adsorption configuration, respectively, which can be determined by Eqs. (S6)-(S8) in Table S1. They are however expected to be lower than the corresponding binding energies for the isolated AX_m and $BY_{m'}$ radicals, due to the intramolecular interaction between A and B atoms in the AX_m-$BY_{m'}$ molecule. Therefore, a different classification of bond strength is considered here to estimate the $Q_{A\text{-}M}$ and $Q_{B\text{-}M}$. Generally, radicals with a closed electronic shell or just one unpaired electron are taken as weak binding, such as CH_2 in CH_2CH; Bond strength of CH in CH_2CH is considered as medium, which has one unpaired electrons and one π bond; Species with two or more than two unpaired electrons are considered as strong binding, like C in CCH_2.

By adopting the modified UBI-QEP formulas (equations introduced above and in Table 1), a comparison between the adsorption heats estimated by improved UBI-QEP approach and that of the DFT (BEEF-vdW) calculations on the most close-packed Co, Ru, Fe, Ni, Cu, Rh, Pd and Pt surfaces are shown in Figure 2b, with a mean absolute error (MAE) of 0.17 eV. The improved UBI-QEP approach estimated binding energies satisfactorily fit with the DFT predicted values and exhibits a simpler formula but higher accuracy as compared to the standard UBI-QEP method (MAE: 0.63 eV). Despite the acceptable overall accuracy, some of the points on Cu (111) surface are observed to deviate from the fitted line farther than others. Therefore, more studies are necessary in future to further improve the UBI-QEP method towards adsorption energies on Cu, possibly also over Ag and Au surfaces. Interestingly, the improved UBI-QEP models can be satisfactorily extended to more open surfaces (211) and (100). A good relationship with the DFT predicted adsorption heats is observed in Figure 2c (MAE: 0.17 eV). The results suggest that the improved UBI-QEP model can be applied to various surfaces of different transition metals.

To further verify the accuracy of the modified UBI-QEP approach, the estimated binding energies of CO, CH_4, C_2H_6, C_3H_8, H_2O, CH_3OH, CH_3, CH_2, CH, H, OH, OCH_3 and O(O)CH species are compared with the experimental results reported by Campbell and co-workers,[43–45] shown as the blue triangles (MAE: 0.13 eV) in Figure 2d. The black circles correspond to the correlation of DFT values against experiment (MAE: 0.16 eV). Through comparison, it can be found that the UBI-QEP results match the experimental values even better than DFT, especially for CO adsorption, points in the range of 1–2 eV, and adsorption of species with binding energies greater than 3 eV, revealing a high accuracy of the modified UBI-QEP method. To sum up, by using both DFT (BEEF-vdW) and experimental values as benchmarks, the modified UBI-QEP method exhibits a reasonable degree of accuracy, which can be utilized to rapidly predict adsorption heats over various transition metal surfaces.

Prediction of activation energy

Besides the quick prediction of adsorption energies, the UBI-QEP method also provides a simplified solution to rapidly estimate the activation energies on transition-metal surfaces. However, an accurate treatment of transition state bond index remains difficult, which results in a poor accuracy of the standard UBI-QEP method compared to DFT (BEEF-vdW) calculations, as shown in Figure S3a and S3b (See Supplementary Information Part S1). Despite several optimization processes attempted to improve the accuracy of UBI-QEP method, the desired accuracy is not achieved. Therefore, another commonly used approach, the BEP relationship, is utilized here to aid the fast prediction of activation energies.

To identify homologous series, a preliminary testing is conducted and shows that the C-H, C-O, C-C, and O-H bond activation are the possible reaction types towards molecules and fragments of interest. The detailed classification is defined as (1) C-H bond cleavage. Reactions of this class correspond to the bond breaking of C-H in fragments like C_xH_y, H_xCO, and H_xCOH; (2) C-O bond cleavage. Into this type fall C-O bond breaking in CO_2, COOH, COH, H_xCOH and H_xCO; (3) C-C bond cleavage. This class comprises C-C bond breaking in hydrocarbon and radicals that including 2 or more than 2 carbon atoms; (4) O-H bond recombination. H_2O, OH, COH, H_xCOH and COOH formation via O-H bond association belongs to reactions of this class. Based on the microscopic reversibility principle,[46] the relationship between forward activation energy (E_f), reverse activation energy (E_r) and the reaction enthalpy (ΔH) is described as $E_f = E_r + \Delta H$. Therefore, the activation energies of the C-H, C-O, C-C bond recombination and the O-H bond cleavage reactions can easily be determined by establishing the BEP relationships for the aforementioned reactions. These relationships are derived based on the DFT calculated activation energies and reaction heats, as displayed in Figure 3a. Their corresponding linear regression equations are defined as

$$E_a = 0.89\Delta H + 0.75 \quad (15)$$

$$E_a = 0.65\Delta H + 1.21 \quad (16)$$

$$E_a = 0.89\Delta H + 0.98 \quad (17)$$

Where Eq. (15) and (16) describe the C-H and C-O bond cleavages, respectively, and the slopes of 0.89 and 0.65 indicate the 'product-like' transition states. For O-H bond recombination (Eq. 17), the slope is 0.89, and value of 0.11 is predicted as the slope for reverse reactions, indicating 'reactant-like' transition states for O-H bond cleavage. Thus, towards above three type reactions, through model fitting, general BEP relationships

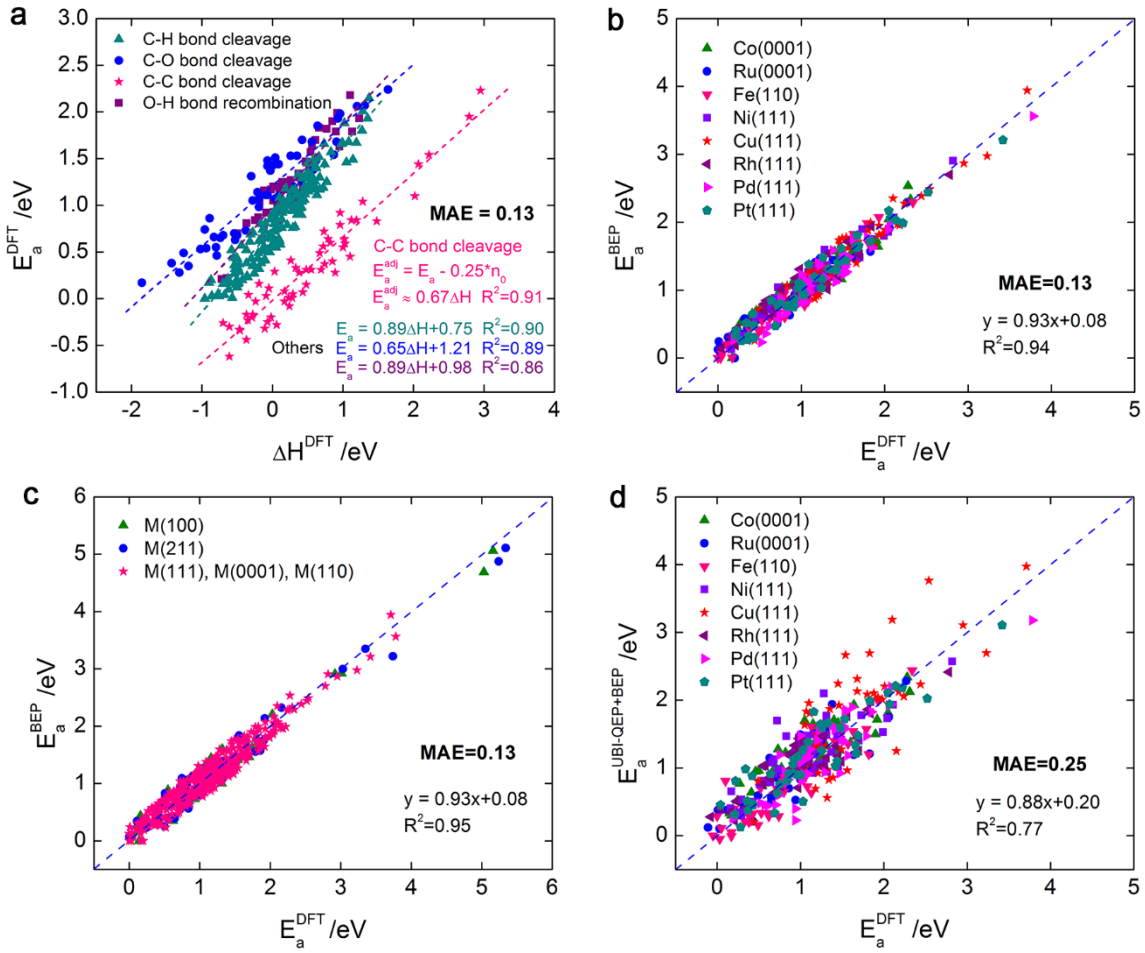

Figure 3. a, DFT (BEEF-vdW) calculated activation energies as a function of reaction heats for C-H, C-O, C-C bond cleavage and O-H bond recombination on the most close-packed surfaces of Co, Ru, Fe, Ni, Cu, Rh, Pd and Pt; b, DFT+BEP estimated activation energies versus DFT (BEEF-vdW) values on the most close-packed surfaces of Co, Ru, Fe, Ni, Cu, Rh, Pd and Pt; c, DFT+BEP estimated activation energies versus DFT (BEEF-vdW) values on M(100), M(211), M(111), M(0001) and M(110) surfaces. M represents for Co, Fe, Pt, Pd, Ru, Rh, Ni, Cu, Ag and Au; d, UBI-QEP+BEP estimated activation energies versus DFT (BEEF-vdW) values across Co(0001), Ru(0001), Fe(110), Ni(111), Cu(111), Rh(111), Pd(111) and Pt(111) surfaces.

(constant α_0 and β_0) are gained, which would be used in the future for fast prediction of activation barriers.

C-C bond cleavage is, however, a special case, and due to the non-uniform linear relationship for all metals together, the BEP relationships can be divided into three parts: Pt; Ru, Rh, Pd; and Fe, Co, Ni, Cu. As shown in Figure S4c, the slopes for all three scaling relations are similar, while their intercepts have certain differences. One of our interesting findings in this study is that we found a correlation between the BEP intercepts (φ) and the period numbers (n_0) of these metals in the periodic table. For example, Pt with the period number of 6, has the highest intercept, 1.58; Ru, Rh and Pd have the intercept of 1.23, with 5 as period number; and Fe, Co, Ni, and Cu with the lowest period number, 4, have the lowest value of intercept, 0.95. Consequently, an average value of $\varphi/n_0 \approx 0.25$ is obtained, and accordingly we proposed the $0.25n_0$ as the intercept for the BEP relationship of C-C bond cleavages. To test and verify that, adjusted activation barriers, $E_a - 0.25n_0$, are applied to generate the new scaling, shown as Figure 3a, which exhibits a much better relationship. The new slope is around 0.67, and the new intercept is about 0, proving the guess. Consequently, this type of reactions could be determined by:

$$E_a = 0.67\Delta H + 0.25n_0 \quad (18)$$

The phenomenon that period number influences activation energy may be related to the d-band center of different period metals. Figure S6 gives the average d-band center (ε_d) of VIIIB metals as a function of period number (n_0), indicating that the larger the n_0, the more negative the d-band center, the higher the activation barrier. Therefore, activation energy is inversely proportional to the metal d-band center for C-C dissociation reactions, which is in agreement with the result reported by Hammer and Nørskov[47] towards dissociation reactions.

There are however several exceptions that didn't fit with the four aforementioned classification of reactions, i.e. CO

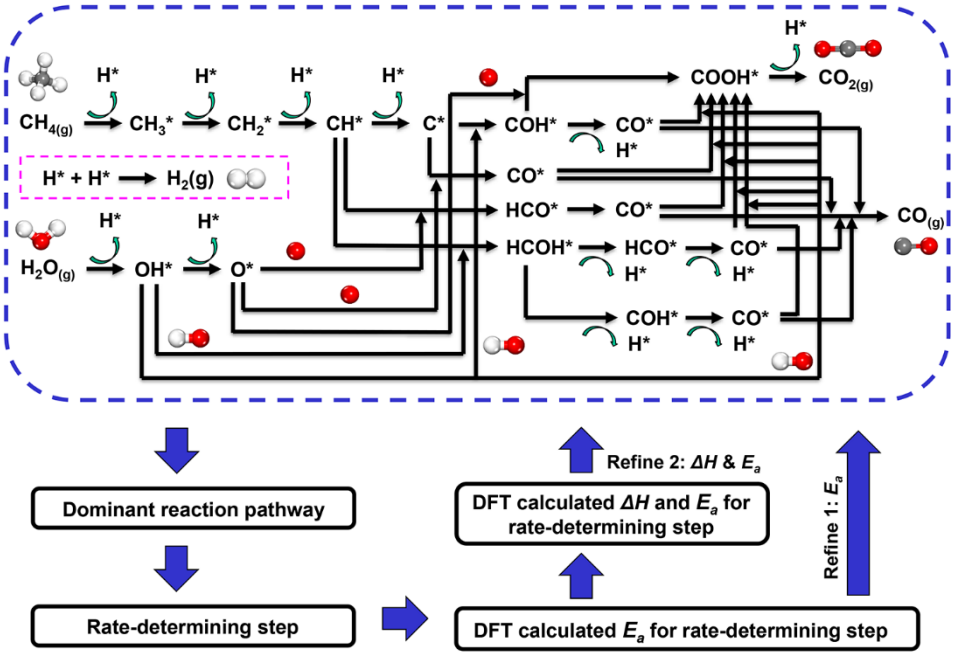

Figure 4. Reaction network of SMR and model refinement. Repeat the loop until convergence: Microkinetic modeling → Dominant reaction pathway → Rate-determining step (RDS) → DFT calculated RDS → microkinetic modeling. Two refined methods are employed. Refine 1: activation energy (Ea) of RDS is calculated by DFT computations. Refine 2: Both activation energy (Ea) and reaction heat (ΔH) of RDS are determined by DFT calculations.

dissociation (CO* → C* + O*), CO* + OH* → COOH*, CH_3* + OH* → CH_3OH* and CH_3* + CH_3* → CH_3CH_3*. Thus separate BEP relationships are generated for those reactions, as described in Supplementary Information Part S2.

The BEP relationships are established based on the most close-packed surfaces. To check whether other metal surfaces such as steps (211) and square-packed (100) surfaces follow the same BEP relationships, we summarized new BEP relationships for three types of reactions on M(100), M(211), M(111), M(0001) and M(110) surfaces. As shown in Figure S7 (See Supplementary Information Part S2), the new BEP relationships are found similar to previous ones. Consequently, we can assume that different metal surfaces follow the same BEP relationships. The BEP relationships on the most close-packed surfaces can be applied for other metal surfaces for fast prediction of activation energies, further aid in rational catalyst design.

Figure 3b gives the activation energies obtained by BEP relationships (in combination with DFT calculated reaction heats) against DFT (BEEF-vdW) values for 50 elementary steps over the most close-packed surfaces of Co, Ru, Fe, Ni, Cu, Rh, Pd and Pt, which illustrates a good linear relationship, MAE: 0.13 eV. The same BEP relationships are subsequently utilized for M(211) and M(100) surfaces, exhibiting a good scaling relation between BEP results and DFT values (MAE: 0.13 eV), as shown Figure 3c. As a result, the applicability of BEP relationships is satisfactorily confirmed. Using the established BEP relationships, it is possible to derive activation energies for heterogeneous reactions merely from reaction heats. Adsorption heats, on the other hand, can be estimated via the improved UBI-QEP method. Since the improved UBI-QEP method and the established BEP relationships have already exhibited a reasonable degree of accuracy separately, the remaining question is that whether the combined UBI-QEP and BEP approach could keep the accuracy. In order to verify the conjecture, we recalculated the activation energies based on the UBI-QEP estimated adsorption heats, and the BEP relationships across Co(0001), Ru(0001), Fe(110), Ni(111), Cu(111), Rh(111), Pd(111) and Pt(111) surfaces. The corresponding activation energies are plotted versus DFT (BEEF-vdW) calculated ones, as shown in Figure 3d, with a MAE of 0.25 eV. Even though the MAE of the improved UBI-QEP + BEP is larger than the improved UBI-QEP (0.17 eV), and BEP relationships (0.13 eV), separately, the value is acceptable, as compared to previously published work.[48–50] It can be also concluded that although more subdivisions of adsorbate and bond types are added in the modified equations, leading to increased complexity, the accuracy has been greatly improved as compared to standard equations. Therefore, the strategy that using improved UBI-QEP + BEP to generate energetics for transition metal surface reactions is proposed here, which is a feasible way to quickly and reasonably gain the input parameters of microkinetic model, so as to achieve the purpose of catalyst prediction.

Microkinetic modeling of SMR

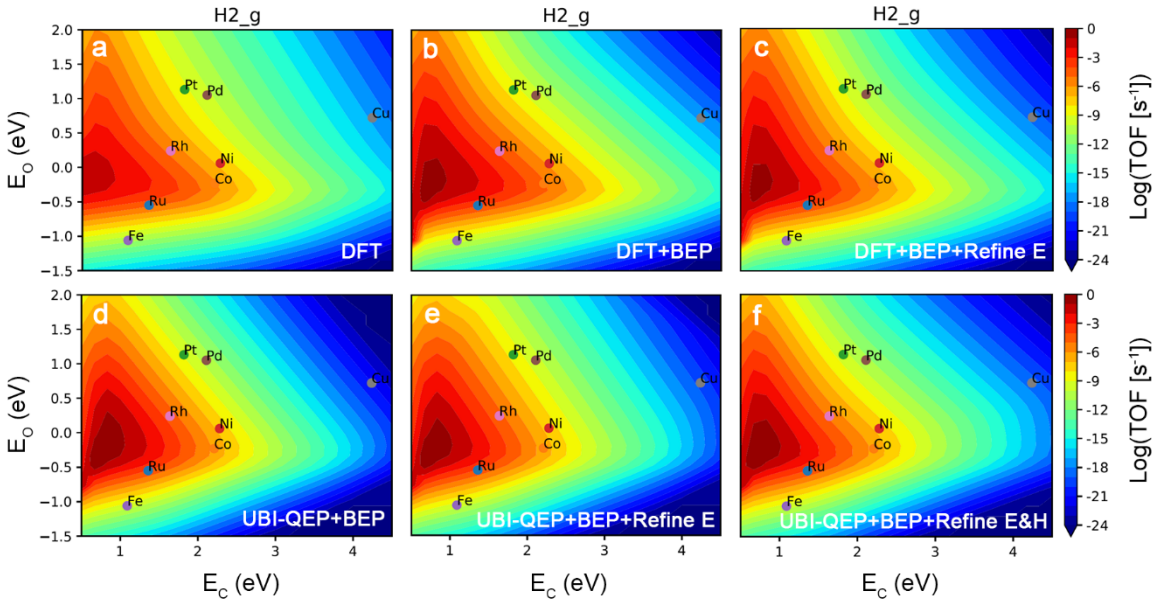

Figure 5. Calculated log(TOF) for H_2 production in steam methane reforming over Co(0001), Ru(0001), Fe(110), Ni(111), Cu(111), Rh(111), Pd(111) and Pt(111) surfaces, under conditions: T = 773 K, P = 1 bar, with a gas composition of 18.2% CH_4, 63.6% H_2O, 18.2% H_2. a, DFT data; b, DFT+BEP (DFT calculated adsorption heats combined with BEP relationships estimated activation energies); c, DFT+BEP+Refine E (DFT+BEP, activation barrier of RDS is estimated by DFT computations); d, UBI-QEP+BEP (improved UBI-QEP calculated adsorption heats combined with BEP relationships estimated activation energies); e, UBI-QEP+BEP+Refine E (improved UBI-QEP+BEP, activation barrier of RDS is estimated by DFT computations); f, UBI-QEP+BEP+Refine E&H (improved UBI-QEP+BEP, activation barrier and reaction heat of RDS are estimated by DFT computations).

A simple reaction, steam methane reforming (SMR) was taken as a tentative reaction to test and verify the applicability of the improved scaling relations. Here SMR reaction involves not only $CH_4 + H_2O \rightarrow H_2 + CO$, but also water gas shift reaction (WGS: $H_2O + CO \rightarrow H_2 + CO_2$), due to the phenomenon that SMR is normally accompanied by WGS under realistic experimental conditions. The total reaction of $CH_4 + H_2O \rightarrow H_2 + CO + CO_2$ is therefore taken into account in this model. The reaction mechanisms are displayed in Supplementary Information Part S4. Figure 4 gives the reaction network of SMR, which exhibits a slight complexity although only 12 intermediates are involved. As for other complex reactions, such as steam ethanol reforming, steam acetic acid reforming and Fischer-Tropsch synthesis, hundreds of intermediates might be involved, thus using improved UBI-QEP + BEP to quickly predict the energetics and do mechanism reduction based on microkinetic modeling is essential and a good strategy.

In the view of which the majority of kinetic parameters in a microkinetic model are not important,[51] the improved UBI-QEP + BEP can be utilized to generate the initial approximations for all parameters. These parameters are subsequently applied to conduct the microkinetic study, and identify the dominant reaction pathway through comparing the reaction rates of elementary steps. The one owing the highest net reaction rate is considered as the dominant reaction route, in which the elementary step with lowest forward reaction rate is the rate-determining step (RDS). Once the important kinetic parameters (energetics in RDS or rate relevant steps) are determined, a more accurate estimation of these parameters can be carried out via DFT calculations in order to refine the model and improve the overall accuracy. Two refined methods are employed here, one is adopting DFT (DFT/BEEF-vdW) to calculate only the activation energies (E_a) for the RDSs, and the other is using DFT to determine both activation energies (E_a) and reaction heats (ΔH) for the RDSs. The new data continues to be utilized for microkinetic modeling, repeating the loop until convergence, shown as in Figure 4. The model sensitivity to RDS is tested by comparison of refine models with unrefined models as well as models between two different refined methods.

Microkinetic modeling is performed by using CatMAP (Catalysis Microkinetic Analysis Package), a software package to describe catalytic trends with descriptor-based microkinetic mapping,[52] which has been widely used in catalytic processes.[40, 41, 53, 54] The simulated reaction condition is T = 773 K, P = 1 bar, with a gas composition of 18.2% CH_4, 63.6% H_2O, 18.2% H_2. In Figure 5 we report the predicted activity as a function of C- and O-metal formation energy for H_2 production in SMR over Co(0001), Ru(0001), Fe(110), Ni(111), Cu(111), Rh(111), Pd(111) and Pt(111) surfaces, with six different methods to obtain surface energetics. Due to the same scaling relations (improved UBI-QEP method and BEP relationships) among different metal facets, the volcano plot obtained from the most close-packed surfaces is suitable for all the surfaces. Comparison of Figure 5a and b demonstrates that using BEP relationships leads to a

slightly higher activity of researched catalysts than using total DFT values. This is caused by BEP estimated lower activation barrier of RDS (CH + O → HCO) than DFT data. In contrast, the refined model (DFT+BEP+Refine E) exhibits a similar TOF level to total DFT model, given as Figure 5c versus Figure 5a. Therefore, implanting DFT computations to calculate the activation energy of RDS is a good approach to improve the model accuracy that is reduced by BEP relationships.

The improved UBI-QEP estimated adsorption energies and BEP calculated activation energies are used as input parameters to conduct microkinetic modeling, with the volcano plot shown as Figure 5d. Additionally, two refined methods, DFT calculated activation barrier of RDS, and DFT calculated activation barrier and reaction heat of RDS, are employed to optimize the model combining with the improved UBI-QEP + BEP method and the results are shown as Figure 5e and f, respectively. The obtained volcano plots as well as predicted catalyst activities are almost same regarding Figure 5d, e and f, which are also very close to Figure 5c, indicating a high accuracy of the improved scaling relations. In other words, combination of UBI-QEP method and BEP relationships generates a similar activation barrier of rate-determining step to DFT value here. It is possible, but might be a coincidence. Next, if applying this method to other reaction systems, the model refinement (using DFT computations to calculate activation energy of RDS) might be still necessary in order to improve the overall accuracy. The direct UBI-QEP + BEP model could be applied to rapidly predict the activity tendency.

According to previous studies,[55–57] Ru, Rh, Ni, Pt and Pd are relatively highly active catalysts for steam methane reforming reaction, thus are chosen to be studied. Towards Figure 5 a ~ f, the relative activities among the 5 transition metal catalysts are: Ru ~ Rh > Ni > Pt > Pd, which are consistent with the experimental results[56–59] reported previously. The practicality of the models are therefore proved, and the improved UBI-QEP + BEP could be applied in the first step of catalyst design to rapidly screen highly active transition-metal catalysts. Using the improved scaling relations to fast estimate surface energetics, then adopting DFT computations to calculate the activation energy of RDS is a good strategy to refine the model. In the future, the strategy would be extended to others reaction systems like N-, S-containing species, as well as more kinds of catalysts (e.g., various facets, metals and/or oxides, nitrides).

Conclusions

This work proposes a strategy that using improved scaling relations (UBI-QEP + BEP) to rapidly and effectively design catalyst by microkinetic modeling using fast estimated energetics of $C_xH_yO_z$ adsorption and surface reactions over transition-metal surfaces. DFT (BEEF-vdW) values on transition metals with different surfaces were utilized as a systematic benchmark to improve the UBI-QEP method to predict the adsorption heat and obtain BEP relationships to estimate activation energies for surface reactions. By taking into account the changes in the molecular structure and A-B bond index during the adsorption, it significantly improved the accuracy of UBI-QEP method to predict the adsorption energy from the atomic binding energies. It satisfactorily fits DFT calculated adsorption energies (MAE: 0.17 eV) and shows an excellent accuracy by comparison with experimental values (MAE: 0.13 eV). BEP relationships are systematically obtained towards C-H, C-O, C-C bond cleavage and O-H bond recombination (MAE: 0.13 eV). Combination of improved UBI-QEP and BEP exhibits an acceptable accuracy with respect to DFT computations (MAE: 0.25 eV). Steam methane reforming is performed as a tentative reaction, for which the catalytic trend predicted by microkinetic modeling is Ru ~ Rh > Ni > Pt > Pd, in good agreement with experimental results. Validity of the improved UBI-QEP + BEP approach is thus proved, which reduces radically six orders of magnitude in the computational expenses (~1 cpu-s for this approach vs. ~320 cpu-h for DFT calculations), but keeps a reasonable degree of accuracy compared to DFT (BEEF-vdW) computations as well as experiments. The rapidly generated energetics is possible to be utilized in the first step of catalyst rational design for fast screening highly active and selective heterogeneous transition-metal catalysts. Moreover, the hybrid microkinetic approach, where microkinetic modeling and analysis is performed firstly by the combined improved UBI-QEP and BEP approach, and the activation energy of the rate-determining step is replaced by the DFT values, can improve the accuracy of the microkinetic modeling and the catalyst prediction.

Methods

DFT calculations

Periodic DFT calculations were performed by using the Vienna Ab-initio Simulation Package (VASP) code.[60–63] The BEEF-vdW exchange-correlation functional,[64] treated with the generalized gradient approximation (GGA),[65] was employed for electron smearing. Interaction between valence electrons and ion cores was described by projector augmented-wave (PAW) method,[66] with plane wave energy cutoff of 400 eV. To achieve convergence, the forces on all unconstrained atoms were less than 0.03 eV/Å. Calculations were processed on Co(0001), Ru(0001), Fe(110), Ni(111), Rh(111), Pt(111), Pd(111), Cu(111), Ag(111), Au(111), Fe(100), Ni(100), Rh(100), Pt(100), Pd(100), Cu(100), Ag(100), Au(100), Ni(211), Rh(211), Pt(211), Pd(211), Cu(211), Ag(211) and Au(211) surfaces. The M(0001), M(110), M(111) and M(100) surfaces were modeled by p(3 × 3) unit cell of five layers. The bottom two layers kept fixed in their crystal positions, while the top three layers and all adsorbates were allowed to relax. The M(211) surfaces were modeled by p(1 × 3) unit cell of 15 layers, with the bottom six layers fixed. A vacuum spacing of 12 Å was built between successive slabs. Brillouin zone sampling was carried out using 5 × 5 × 1 k-point for M(0001), M(110), M(111) and M(100), and 5 × 3 × 1 k-point for M(211) calculations. Dimer method was applied to search for transition states.

Gas phase bond energies were determined by DFT computations. The lattice parameters for gas calculations were a = 20.0 Å, b = 20.5 Å, c = 21.0 Å. BEEF-vdW functional, 400 eV cutoff energy and 0.01 eV/Å force threshold were applied in the

optimization. Brillouin zones sampling was done using a 1 × 1 × 1 Gamma k-point mesh.

Surface energetics

The adsorption energies and activation energies are calculated by:

$$E_{ads} = E_{adsorbate+surface} - E_{adsorbate} - E_{surface} \quad (19)$$

$$E_a = E_{TS} - E_{IS} \quad (20)$$

Where $E_{adsorbate}$ is the gas-phase total energy of adsorbate. $E_{surface}$ is the total energy of a clean metal surface. $E_{adsorbate+surface}$ is the total energy of metal surface with adsorbate adsorbed. E_{ads} is adsorption energy. E_{IS} is the total energy of reactant, E_{TS} is the total energy of transition state, E_a is activation energy.

UBI-QEP method

The assumptions, fundamental category and equations of standard UBI-QEP method are given in Supplementary Information.

Conflicts of interest

There are no conflicts to declare.

Acknowledgements

The supports from NTNU energy, Norwegian research council, the Natural Science Foundation of China (91645122, 21473053, and U1663221), as well as the computational time provided by the Notur project (nn4685k) are highly acknowledged.

Notes and references

1 H. Falsig, B. Hvolbæk, I. S. Kristensen, T. Jiang, T. Bligaard, C. H. Christensen and J. K. Nørskov, *Angew. Chem. Int. Ed.,* 2008, **47**, 4835–4839.
2 P. Ferrin, D. Simonetti, S. Kandoi, E. Kunkes, J. A. Dumesic, J. K. Nørskov and M. Mavrikakis, *J. Am. Chem. Soc.,* 2009, **131**, 5809−5815.
3 A. C. Lausche, A. J. Medford, T. S. Khan, Y. Xu, T. Bligaard, F. Abild-Pedersen, J. K. Nørskov and F. Studt, *J. Catal.,* 2013, **307**, 275−282.
4 J. S. Yoo, F. Abild-Pedersen, J. K. Nørskov and F. Studt, *ACS Catal.,* 2014, **4**, 1226−1233.
5 J. E. Sutton and D. G. Vlachos, *J. Catal.,* 2016, **338**, 273–283.
6 D. Loffreda, F. Delbecq, F. Vigné and P. Sautet, *Angew. Chem.,* 2009, **121**, 9140–9142.
7 K. Honkala, A. Hellman, I. N. Remediakis, A. Logadottir, A. Carlsson, S. Dahl, C. H. Christensen and J. K. Nørskov, *Science* 2005, **307**, 555–558.
8 M. Saeys, M. F. Reyniers, J. W. Thybaut, M. Neurock and G. B. Marin, , *J. Catal.,* 2005, **236**, 129–138.
9 A. A. Gokhale, J. A. Dumesic and M. Mavrikakis, *J. Am. Chem. Soc.,* 2008, **130**, 1402–1414.
10 J. K. Nørskov, T. Bligaard, J. Rossmeisl and C. H. Christensen, *Nat. Chem.,* 2009, **1**, 37–46.
11 M. L. Yang, C. Fan, Y. A. Zhu, Z. J. Sui, X. G. Zhou and D. Chen, *J. Phys. Chem. C* 2015, **119**, 21386–21394.
12 Y. Qi, C. Ledesma, J. Yang, X. Duan, Y. A. Zhu, A. Holmen and D. Chen, *J. Catal.,* 2017, **349**, 110–117.
13 Z. W. Ulissi, A. J. Medford, T. Bligaard and J. K. Nørskov, *Nat. Commun.,* 2017, **8**, 14621.
14 M. Maestri and K. Reuter, *Chem., Int. Ed.,* 2011, **50**, 1194–1197.
15 F. Abild-Pedersen, J. Greeley, F. Studt, J. Rossmeisl, T. R. Munter, P. G. Moses, E. Skúlason, T. Bligaard and J. K. Nørskov, *Phys. Rev. Lett.,* 2007, **99**, 016105.
16 E. Shustorovich, *Surf. Sci. Rep.,* 1986, **6**, 1–63.
17 E. Shustorovich, *Acc. Chem. Res.,* 1988, **21**, 183–189.
18 E. Shustorovich, *J. Mol. Catal.,* 1989, **54**, 301–311.
19 E. Shustorovich and H. Sellers, *Surf. Sci. Rep.,* 1998, **31**, 1–119.
20 E. Shustorovich and A. T. Bell, *Surf. Sci.,* 1991, **248**, 359–368.
21 E. Shustorovich and A. T. Bell, *Surf. Sci.,* 1991, **253**, 386−394.
22 S. Azizian and F. Gobal, *Langmuir* 2000, **16**, 8095−8099.
23 R. S. Vincent, R. P. Lindstedt, N. A. Malik, I. A. B. Reid and B. E. Messenger, *J. Catal.,* 2008, **260**, 37−64.
24 J. Greeley, *Annu. Rev. Chem. Biomol. Eng.,* 2016, **7**, 605−635.
25 M. M. Montemore and J. W. Medlin, *Catal. Sci. Technol.,* 2014, **4**, 3748−3761.
26 E. Vesselli, G. Coslovich, G. Comelli and R. Rosei, *J. Phys. Condens. Matter* 2005, **17**, 6139.
27 E. Shustorovich, *Russ. J. Phys. Chem. B* 2007, **1**, 307−329.
28 a) J. N. Bronsted, *Chem. Rev.,* 1928, **5**, 231−338; b) M. G. Evans and M. Polanyi, *Trans. Faraday Soc.,* 1938, **34**, 11–24.
29 B. Yang, R. Burch, C. Hardacre, G. Headdock and P. Hu, *ACS Catal.,* 2014, **4**, 182–186.
30 A. Michaelides, Z. P. Liu, C. J. Zhang, A. Alavi, D. A. King and P. Hu, *J. Am. Chem. Soc.,* 2003, **125**, 3704−3705.
31 M. Mahmoodinia, T. T. Trinh, P. O. Åstrand and K. Q. Tran, *Phys. Chem. Chem. Phys.,* 2017, **19**, 28596-28603.
32 J. K. Nørskov, T. Bligaard, B. Hvolbæk, F. Abild-Pedersen, I. Chorkendorff and C. H. Christensen, *Chem. Soc. Rew.,* 2008, **37**, 2163−2171.
33 J. K. Nørskov, T. Bligaard, A. Logadottir, S. Bahn, L. B. Hansen, M. Bollinger, H. Bengaard, B. Hammer, Z. Sljivancanin, M. Mavrikakis,; Y. Xu, S. Dahl and C. J. H. Jacobsen, *J. Catal.,* 2002, **209**, 275−278.
34 H. F. Wang and Z. P. Liu, *J. Am. Chem. Soc.,* 2008, **130**, 10996−11004.
35 J. E. Sutton and D. G. Vlachos, *ACS Catal.,* 2012, **2**, 1624−1634.
36 K. Lee, E. Lee, C. Song and M. J. Janik, *J. Catal.,* 2014, **309**, 248−259.
37 E. Shustorovich and A. V. Zeigarnik, *Surf. Sci.,* 2003, **527**, 137−148.
38 E. M. Shustorovich and A. V. Zeigarnik, *Russ. J. Phys. Chem.,* 2006, **80**, 4−30.
39 S. Storsæter, D. Chen and A. Holmen, *Surf. Sci.,* 2006, **600**, 2051−2063.
40 C. A. Wolcott, A. J. Medford, F. Studt and C. T. Campbell, *J. Catal.,* 2015, **330**, 197−207.
41 L. Yu and F. Abild-Pedersen, *ACS Catal.,* 2017, **7**, 864−871.
42 B. H. Bransden and C. J. Joachain, Physics of atoms and molecules Longman Scientific & Technical. 1983.
43 J. Wellendorff, T. L. Silbaugh, D. Garcia-Pintos, J. K. Nørskov, T. Bligaard, F. Studt and C. T. Campbell, *Surf. Sci.,* 2015, **640**, 36−44.
44 C. A. Wolcott, I. X. Green, T. L. Silbaugh, Y. Xu and C. T. Campbell, *J. Phys. Chem. C* 2014, **118**, 29310-29321.
45 S. J. Carey, W. Zhao and C. T. Campbell, *Angew. Chem.,* 2018, **130**, 17119–17123.
46 R. I. Masel and R. I. Masel, John Wiley & Sons 1996, **3**.
47 B. Hammer and J. K. Nørskov, *Adv. Catal.,* 2000, **45**, 71−129.
48 S. Wang, B. Temel, J. Shen, G. Jones, L. C. Grabow, F. Studt, T. Bligaard, F. Abild-Pedersen, C. H. Christensen and J. K. Nørskov, *Catal. Lett.,* 2011, **141**, 370−373.
49 S. Wang, V. Petzold, V. Tripkovic, J. Kleis, J. G. Howalt, E. Skúlason, E. M. Fernández, B. Hvolbæk, G. Jones, A. Toftelund, H. Falsig, M. Björketun, F. Studt, F. Abild-Pedersen, J.

Rossmeisl, J. K. Nørskov and T. Bligaard, *Phys. Chem. Chem. Phys.,* 2011, **13**, 20760−20765.
50 S. Wang, V. Vorotnikov, J. E. Sutton and D. G. Vlachos, *ACS Catal.,* 2014, **4**, 604−612.
51 A. H. Motagamwala, M. R. Ball and J. A. Dumesic, *Annu. Rev. Chem. Biomol. Eng.,* 2018, **9**, 413−450.
52 A. J. Medford, C. Shi, M. J. Hoffmann, A. C. Lausche, S. R. Fitzgibbon, T. Bligaard and J. K. Nørskov, *Catal. Lett.,* 2015, **145**, 794−807.
53 K. Yang and B. Yang, *J. Phys. Chem. C* 2018, **122**, 10883−10891.
54 D. Xu, P. Wu and B. Yang, *J. Phys. Chem. C* 2019, **123**, 8959−8966.
55 G. Jones, J. G. Jakobsen, S. S. Shim, J. Kleis, M. P. Andersson, J. Rossmeisl, F. Abild-Pedersen, T. Bligaard, S. Helveg, B. Hinnemann, J. R. Rostrup-Nielsen, I. Chorkendorff, J. Sehested and J. K. Nørskov, *J. Catal.,* 2008, **259**, 147−160.
56 J. R. Rostrup-Nielsen, *J. Catal.,* 1973, **31**, 173−199.
57 E. Kikuchi, S. Tanaka, Y. Yamazaki and Y. Morita, *Bull. Jpn. Pet. Inst.,* 1974, **16**, 95−98.
58 J. R. Rostrupnielsen and J. H. B. Hansen, *J. Catal.,* 1993, **144**, 38−49.
59 D. Qin and J. Lapszewicz, *Catal. Today* 1994, **21**, 551−560.
60 G. Kresse and J. Hafner, *Phys. Rev. B* 1993, **47**, 558.
61 G. Kresse and J. Hafner, *Phys. Rev. B* 1994, **49**, 14251.
62 G. Kresse and J. Furthmüller, *Comp. Mater. Sci.,* 1996, **6**, 15−50.
63 G. Kresse and J. Furthmüller, *Phys. Rev. B* 1996, **54**, 11169.
64 R. Y. Brogaard, P. G. Moses and J. K. Nørskov, *Catal. Lett.,* 2012, **142**, 1057−1060.
65 J. P. Perdew, K. Burke and M. Ernzerhof, *Phys. Rev. Lett.,* 1996, **77**, 3865.
66 P. E. Blöchl, *Phys. Rev. B* 1994, **50**, 17953.

